RZ 3544 (# 99563) 08/23/04
Electrical Engineering 39 pages

Research Report

Impact of the FCC Average- and Peak Power Constraints on the Power of UWB Radio Signals

Martin Weisenhorn and Walter Hirt

IBM Research GmbH
Zurich Research Laboratory
8803 Rüschlikon
Switzerland

Contents

Abstract

UWB radio signals for communication and/or position location have an extremely low power spectral density, such that other devices, in particular narrowband radio receivers, experience only a marginal performance degradation, if any. The binding regulation for the emission limits of UWB radio devices released by the FCC consists essentially of the allowed frequency range as well as *average*, and *peak-power* constraints. In this paper we investigate the impact of these constraints on the maximum emission power-spectral-density of UWB radio signals for different modulation schemes by both, analysis and simulation. We point out that for a given signal, the peak power constraint may or may not be active, depending on the resolution bandwidth used to measure the peak power; the reasons for this as well as solutions to avoid this dependency are proposed. New insights on the requirements for achieving spectral flatness of UWB signals are obtained.

Keywords: Average power, peak power, FCC power constraints, bandwidth scaling factor, UWB signals.

Glossary

BPSK	Binary Phase Shift Keying
DSSS	Direct-Sequence Spread-Spectrum (DS-UWB)
DS	Direct Sequence
EIRP	Effective Isotropic Radiated Power
ESD	Energy Spectral Density
FCC	Federal Communications Commission
IF	Intermediate Frequency
iid	Independent Identically Distributed
NBW	Noise Bandwidth
NTIA	National Telecommunications and Information Administration
OFDM	Orthogonal Frequency Division Multiplexing
PAPR	Peak-to-Average Power Ratio
PDF	Probability Density Function
PPM	Pulse Position Modulation
PRF	Pulse Repetition Frequency
PSD	Power Spectral Density
RBW	Resolution Bandwidth
SF	Scaling Factor
US	United States
UWB	Ultra-Wideband
2PAM	Binary Antipodal Modulation
2PPM	Binary Pulse Position Modulation

1 Introduction

To test an ultra-wideband (UWB) radio transmitter for compliance with the emission rules issued by the United States (US) Federal Communications Commission (FCC) [1], the emitted signal strength, $v(t)$ is measured at a distance of 3 m from the transmitting antenna. This instantaneous signal strength, measured in terms of Volt per meter (V/m), can be translated into an equivalent instantaneous signal power, $s^2(t)$, measured in terms of Watt, where $s(t)$ is the signal at the feed point of an ideal isotropic radiator (antenna): $v(t) = \sqrt{Zs^2(t)/(4\pi r^2)}$, where Z is the wave impedance of the propagation medium and r is the separation between the transmitting antenna and the antenna used to measure the signal strength (see also [2]). The signal $s^2(t)$ is the instantaneous effective isotropic radiated power (EIRP); the average- and peak power constraints specified by the FCC refer to the signal $s(t)$.

Average Power Constraint: The average EIRP is measured with a spectrum analyzer with the resolution bandwidth (RBW) set to 1 MHz; the resulting power that passes the resolution filter is averaged over a 1 ms time window. For all center frequencies of the resolution filter within the communication band 3.1 - 10.6 GHz, this averaged power must be below the limit of -41.25 dBm. Roughly speaking, the measured power spectral density (PSD) must not exceed the level of -41.25 dBm/MHz [1]. For example, a transmitter that exploits the entire available bandwidth of 7.5 GHz may produce an average EIRP of at most 562 μW (or, equivalently, -2.5 dBm).

Peak Power Constraint: The peak of the signal power is measured with a spectrum analyzer with the RBW set to a value between 1 and 50 MHz [1]; the recommended RBW is 3 MHz. This measurement setup is equivalent to a bandpass filter with a corresponding bandwidth followed by an envelope detector, a lowpass filter and a peak detector; the measured peak power level must be below $(\text{RBW}/50\text{ MHz})^2$ mW for all center frequencies of the resolution filter within the communication band of 3.1 - 10.6 GHz. For example, with an RBW of 50 MHz, the instantaneous (peak) power must not exceed 1 mW (or, equivalently, 0 dBm).

The National Telecommunications and Information Administration (NTIA) of the US Department of Commerce documents average- and peak power measurements for UWB signals [2, 3]. The corresponding results are summarized in Fig. 1, showing the peak-to-average power ratio as a function of the signal's pulse repetition frequency (PRF) or R_p, for a series of (i) identical and equidistant pulses, denoted a *non-dithered* signal, and (ii) time-hopped pulses, denoted a *dithered* signal. For dithered signals, the pulse delay varies randomly with a uniform distribution between 0 percent and 50 percent of the average interpulse period. The reasons for the various break points shown in Fig. 1 will become clear subsequently.

The duration of the averaging window to determine the average power is set to 1 ms by the FCC, thus meaningful measurement results for pulsed UWB signals can only be achieved if their PRF is larger than about 10 KHz, see also Subsection 4.1. Correspondingly, in [1, 2, 3], as well

as in this report, the average power of pulsed UWB signals is only evaluated for $R_p \geq 10$ KHz.

Given a certain signal modulation scheme, we are interested in the maximally allowed average or peak EIRP, such that both, the peak- and average power are within their defined limits. From the peak-to-average power ratio (PAPR) alone it is not possible to determine the allowed EIRP, therefore, the absolute values of the peak- and average power limits must be known[1]. In this paper we determine the absolute values for the average- and peak power for different modulation schemes to determine the PRF region for UWB signals that allows to transmit with the highest signal power or energy per transmitted pulse, while satisfying the FCC emission limits. In Section 2 we define the signal model and Section 3 describes the radio sinals for different modulation schemes; the average power is derived analytically and computed numerically in Section 4. Section 5 presents numerical values of the peak power for different modulation schemes based on the results of Section 4 and on the peak-to-average power ratio reported by the NTIA. Section 6 discusses the practical implications of the peak- and average power constraints on the allowed transmitted power. A key parameter for the peak power measurement is the RBW, the bandwidth in which the peak power is determined. The FCC proposed to use any RBW in the range of 1 to 50 MHz and a scaling factor to compensate for different RBWs. However, our results show that the effective peak power constraint depends on the spectrum analyzer's RBW and details of the modulated UWB signal under test. This method results in an unfair power limitation for certain modulation schemes when the RBW used for the peak power measurement is less than 50 MHz. In Section 7 two alternatives are proposed to solve this problem and conclusions are given in Section 8.

2 Signal Model

The FCC suggests to use a spectrum analyzer to measure average- and peak power of an UWB signal. The signal processing scheme of a spectrum analyzer that is adjusted for these measurements can be approximated by the mathematical model visualized in Fig. 2. The tested UWB signal, $s(t)$, is applied to the input of the spectrum analyzer. The classical type of a spectrum analyzer has a heterodyne architecture, which mixes the input signal with a locally generated cosine signal with frequency f_m to a lower intermediate frequency (IF); the mixer product is then filtered by the resolution filter with transfer function $F(f)$. The resolution filter is a bandpass filter with center frequency f_0 equal to the IF. The output signal of this filter, $y(t)$, is passed through an envelope detector; however, the envelope of the signal is independent of the IF, there-

[1]Originally the PAPR was introduced to allow an easy estimation of the peak power by only measuring the average power of a signal [2], however, the corresponding peak-to-average power ratio depends on several modulation parameters, which requires a table of PAPRs with an entry for the current set of modulation parameters.

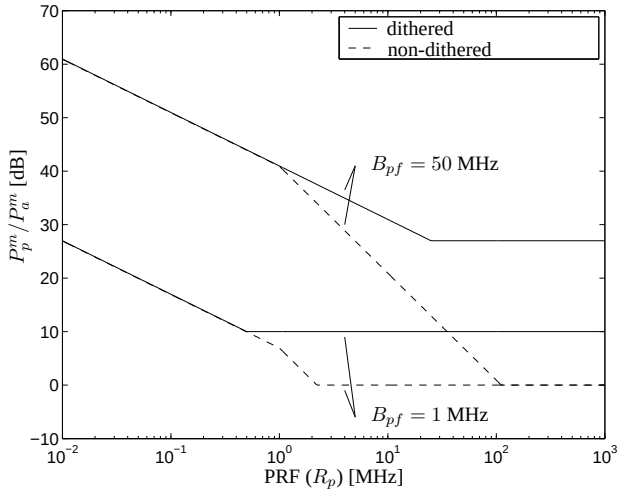

Figure 1: Peak-to-average power ratio as determined by the NTIA [3]; B_{pf} is the RBW.

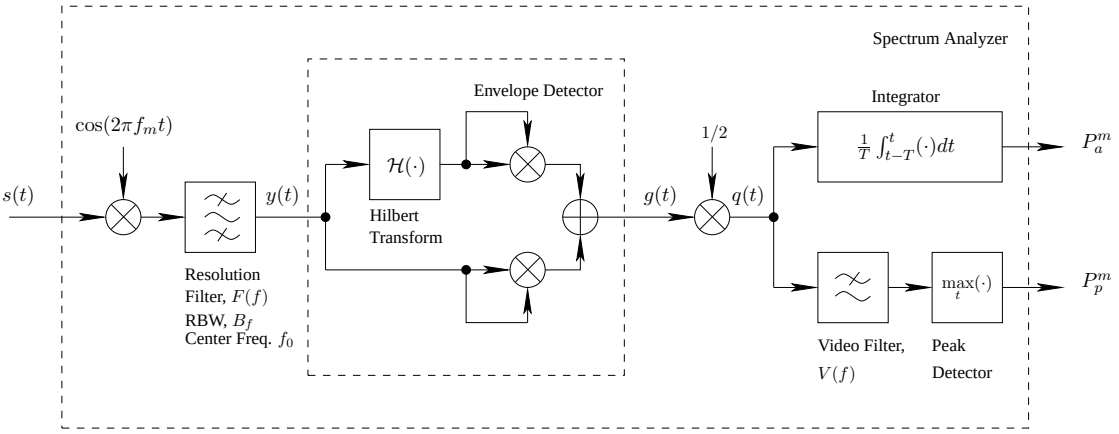

Figure 2: Model of the signal flow in a spectrum analyzer used to measure peak- and average power.

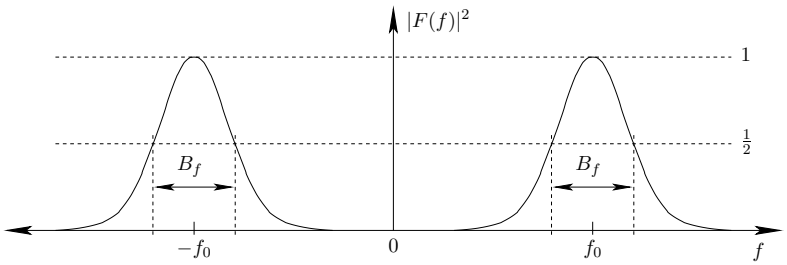

Figure 3: Squared spectrum of a resolution filter with Gaussian magnitude spectrum.

fore for the purpose of analysis and simulation, the input mixer shown in Fig. 2 is not required and we can set $f_m = 0$.

2.1 Resolution Filter

For typical spectrum analyzers, the squared amplitude spectrum of the resolution filter can be approximated by a Gaussian function as shown in Fig. 3. Note that the phase spectrum of the resolution filter is not linear if the impulse response of the IF filter is causal. However, because of lack of better information we assume that the phase spectrum is zero, i.e., the baseband representation of the filter's frequency response and its impulse response are given by

$$F_l(f) = 2e^{-\pi a^2 f^2} \;\bullet\!\!-\!\!\circ\; f_l(t) = \frac{2}{a} e^{-\pi \frac{t^2}{a^2}} \quad .$$

The 3 dB attenuation bandwidth, B_f, specifies a as

$$a = \frac{\sqrt{2\ln(2)}}{\sqrt{\pi} B_f}$$

and the impulse response of the resolution filter is

$$\begin{aligned} f(t) &= \Re\left\{ f_l(t) e^{i2\pi f_0 t} \right\} \\ &= B_f \sqrt{\frac{2\pi}{\ln(2)}} \cos(2\pi f_0 t) e^{-\frac{(\pi B_f t)^2}{2\ln(2)}} . \end{aligned} \tag{1}$$

This impulse response has infinite support; for simulation purposes the impulse response is truncated at $f = xB_f$, with x chosen such that

$$F_l(0) = nF_l(xB_f).$$

Solving this equation for x yields

$$x = \sqrt{\frac{\ln(2n(2\ln(2)\pi)^{1/4})}{2\ln(2)}},$$

where, for example, $n = 1000$ results in $x = 2.31$.

If white noise with a two-sided PSD of $N_0/2$ is applied to this filter, the power at its output is $1.064 N_0 B_f$. Thus, for an ideal bandpass filter with the same input signal, to show the same output power, it must have the bandwidth $B = 1.064 B_f$, i.e., the equivalent noise bandwidth (NBW) of the Gaussian filter is $B_{\text{NBW}} = 1.064 B_f$. For the equivalent NBW of practical spectrum analyzers see [4].

For convenience, the RBW, B_f, will be denoted by B_{af} when used in the context of average power measurements and by B_{pf} in the context of peak power measurements. Average power measurements are performed exclusively with a RBW of $B_{af} = 1$ MHz, while the RBW used for peak power measurements, B_{pf}, can be chosen between 1 to 50 MHz [1].

2.2 Envelope Detector

The filtered signal $y(t)$ enters the envelope detector, which can be mathematically expressed using the Hilbert transform $\mathcal{H}(.)$; the square of the envelope of $y(t)$ is

$$g(t) = y^2(t) + \mathcal{H}^2(y(t)).$$

2.3 Average Power Detector

The RBW will be chosen in the range of 1 - 50 MHz and will thus be much smaller than the signal's main response, which is in the range of 3.1 - 10.6 GHz. Hence, the signal $y(t)$ fed to the envelope detector is a sine function with an amplitude that is approximately constant over several cycles. This allows to approximate the average power of the signal $y(t)$ by $q(t) = g(t)/2$, which is the average taken over the duration of a single cycle. The measurement procedure defined by the FCC to determine the average signal power yields

$$P_a^m = \frac{1}{T} \int_0^T q^2(t) dt,$$

with the period $T = 1$ ms used to average the signal power [1].

We introduce an additional power spectral density measure, D_a, which is the ratio of the total emitted average signal power over the total signal bandwidth, B, i.e.,

$$D_a = \frac{\lim_{T \to \infty} \frac{1}{T} \int_{-T/2}^{T/2} s^2(t) dt}{B},$$

where the units of B and D_a are MHz and W/MHz, respectively. Provided that P_a^m is constant for all center frequencies f_0 of the resolution filter within the signal's spectrum, we have $P_a^m = 1.064\ D_a$ MHz; this is because the equivalent noise bandwidth of the Gaussian resolution filter

is $B_{\text{NBW}} = 1.064B_{af}$ (see Subsection 2.1). The FCC specifies that P_a^m must be below the limit of $P_a = -41.25$ dBm/MHz for all center frequencies f_0 of the resolution filter; therefore, the highest possible transmitted power is reached if P_a^m is independent of f_0, i.e., if the measured signal spectrum is constant.

2.4 Peak Power Detector

Based on the spectrum analyzer schematic displayed in Fig. 2, the peak power is determined by passing half of the the squared signal envelope, i.e, $q(t)$, through the video filter followed by a peak detector. In this analysis we assume a Gaussian lowpass video filter with transfer function $V(f)$, where the 3 dB attenuation bandwidth[2] is set to $4B_{pf}$ (B_{pf} is the RBW of the IF filter). When lower video bandwidths are used, the measured peak power level P_p^m decreases, a video bandwidth of $4B_{pf}$ was chosen to eliminate the impact of the video filter. For the purpose of this analysis, the duration[3] for which the peak detector observes the signal is set to 0.1 ms. This duration is a compromise to allow enough observation time for the peak power simulation and to avoid excessive simulation times.

3 Modulation Schemes

In this Section we define the radio signals for different modulation schemes as they will be used for analysis and simulation to describe the effects of various modulation parameters.

3.1 Pulse Based Modulation Schemes

For pulse based modulation schemes, the one-sided energy spectral density (ESD) per transmitted pulse is set to the value

$$E_{s,p}^t = 10^{-5} \text{ nWs/MHz}.$$

For a PRF of $R_p = 10$ MHz the average PSD of the signal $s(t)$ is thus $D_a = E_{s,p}^t R_p = 100$ nW/MHz $\equiv -40$ dBm/MHz. This particular value is used because it is very close to the FCC average EIRP spectral density limit of -41.25 dBm/MHz $\equiv 75$ nW/MHz and at the same time it is a power of 10, which allows for easy conversion. Note that with this definition of $E_{s,p}^t$ a PSD level of -41.25 dBm/MHz is achieved for a PRF of $R_p = 7.5$ MHz, see also Fig. 4(b) or 4(d).

For the present purpose it is possible to represent UWB pulses by Dirac delta pulses because the spectrum of an UWB pulse can be assumed to be constant within the passband of the

[2] In [1] the FCC requests that the video bandwidth is not less than the RBW of the IF filter.

[3] No statement about the peak power observation time is made in [1].

resolution filter. Note that the RBW B_{pf} varies between 1 MHz and 50 MHz for peak power measurements and $B_{af} = 1$ MHz for average power measurements.

With this, the mathematical expression of a UWB pulse with one-sided energy spectral density $E^t_{s,p}$ becomes $\sqrt{E^t_{s,p}/2}\,\delta(t)$, where $\delta(t)$ is the Dirac delta function. Modeling UWB pulses by Dirac delta pulses, yields accurate results, as long as exclusively in-band emission is considered, which is the case in this paper. Furthermore, UWB pulses can be modelled by Dirac delta pulses only if their energy spectrum is constant within the considered frequency band. For this study we assume that this is satisfied; therefore, our results can be interpreted independent of specific pulse shapes. Out-of-band emission is determined by the signal's frequency spectrum and thus by the detailed shape of the UWB pulses. Hence, when considering out-of-band emission, the pulsed signals defined subsequently must be convolved with the corresponding pulse shapes.

3.1.1 Periodic Stream of Pulses

A periodic stream of pulses is a sequence of equidistant and identical pulses, which we describe as

$$s(t) = \sqrt{\frac{E^t_{s,p}}{2}} \sum_{k=-\infty}^{\infty} \delta(t - k/R_p). \tag{2}$$

This type of signal is denoted as a *non-dithered* signal in [3].

3.1.2 Binary Antipodal Modulated Stream of Pulses

Modulating the sign of the pulses in (2) by data symbols $a_k \in \{-1, +1\}$ results in a binary phase shift keyed (BPSK) or binary antipodal modulated (2PAM) stream of pulses, described as

$$s(t) = \sqrt{\frac{E^t_{s,p}}{2}} \sum_{k=-\infty}^{\infty} a_k \delta(t - k/R_p), \tag{3}$$

where it is assumed that the symbols a_k are independent, identically distributed (iid) binary digits.

3.1.3 Time-Hopped Stream of Pulses

We use a pulse position modulated (PPM) signal with two allowed pulse positions, i.e., a 2PPM signal, the value of the symbol a_k determines at which of the two positions the k-th pulse is transmitted, i.e, the time-hopped stream of pulses is described as

$$s(t) = \sqrt{E^t_{s,p}} \sum_{k=-\infty}^{\infty} \delta[t - k/R_p - a_k/(2R_p)],$$

where the binary symbols $a_k \in \{0, +1\}$ are iid. This modulation scheme is also denoted as 2PPM. What in [3] is denoted as a *dithered signal* corresponds to a PPM signal that is modulated by continuous valued symbols, $a_k \in [0, 1]$.

3.1.4 Combined Binary Antipodal and Time-Hopped Stream of Pulses

This modulation scheme combines 2PAM with 2PPM; the modulated signal is described by

$$s(t) = \sqrt{E^t_{s,p}} \sum_{k=-\infty}^{\infty} a_k \delta(t - k/R_p - b_k/(2R_p)),$$

the symbol streams a_k and b_k are iid with $a_k \in \{-1, +1\}$, and $b_k \in \{0, +1\}$.

3.1.5 Direct-Sequence Spread-Spectrum

We use the direct-sequence spread-spectrum (DSSS) modulation scheme defined in [5], where it is also called DS-UWB. For our purpose it suffices to consider the signal in the low band. This signal is the sum of the signals of six channels which are located in overlapping subbands. We choose a data rate of approximately 110 Mb/s per channel, i.e., a total data rate of approximately 660 Mb/s. The chip rates of these channels are

$$(f_{c,1}, \ldots, f_{c,6}) = (1300, 1313, 1326, 1339, 1352, 1365)$$

MHz; the center frequencies of the respective subbands correspond to three times the chip rates. Because of the simplicity of the employed spreading sequence[4] and the small measurement bandwidth of at most 50 MHz, for our purpose the DSSS signal becomes

$$s(t) = \sqrt{\frac{E^t_{s,p}}{2}} \sum_{n=1}^{6} \sum_{k=1}^{\infty} a_{k,n} \delta(t - kLT_{c,n}),$$

where $T_{c,n} = 1/f_{c,n}$ and $L = 6$ is the length of the spreading sequence; the data symbols $a_{k,n} \in \{-1, +1\}$ are assumed to be iid. In this case the one-sided ESD of a single pulse, $E^t_{s,p}$, is chosen such that the average PSD, $D_a = 75$ nW/MHz $\equiv -41.25$ dBm/MHz, i.e.,

$$E^t_{s,p} = \frac{LD_a}{\sum_{n=1}^{6} f_{c,n}} = 5.6277 \cdot 10^{-8} \text{ nW/MHz}\,.$$

If only one of the six available channels is transmitting with a data rate of 110 Mb/s, the DSSS modulated signal is described by the binary antipodal modulated signal (BPSK or 2PAM) defined above, with the PRF set to a value $f_{c,n}/6$, with $1 \le n \le 6$.

[4] For data rates of 110 Mb/s, the spreading sequence is $(1, 0, 0, 0, 0, 0)$.

3.2 Non-Pulse Based Modulation Schemes

3.2.1 Multiband-OFDM Signal

The multiband orthogonal frequency division multiplexing (OFDM) signal sequence is generated according to [6]; only the payload data within a packet is considered. In our simulation the scrambled data bits are assumed to be iid. We set the duration of the generated data sequence to 1.004 ms, just enough to obtain a signal sequence with a 1 ms duration after IF filtering and after cutting of the transition periods. The guard subcarriers are generated with the same amplitude as the data and pilot carriers. The signal is generated for transmission over Channels 1 and 3 in Band 1 , see [6] Table 15. The frequency-hopping code for Channel 3 causes two OFDM symbols to be transmitted in immediate succession, followed by a mute period with four times the duration of an OFDM symbol. The frequency-hopping code for Channel 1 causes a mute period of twice the duration of an OFDM symbol between successive symbols. The center frequency of the signal in Band 1 is denoted by f_c.

The OFDM signal in [6] is defined in the complex baseband but for our purpose we transform it into passband with center frequency $f_c = 528$ MHz; the power of each subcarrier is 0.5 W. We multiply the OFDM signal with the *amplitude factor* α such that the emitted power per subcarrier divided by the subcarrier-spacing, $\Delta_f = 4.125$ MHz, equals the PSD, of $D_a = 75$ nW/MHz $\equiv -41.25$ dBm/MHz. The duty cycle of the signal is determined by the guard interval $T_{\text{GI}} = 9.47$ ns, the symbol duration $T_{\text{SYM}} = 312.5$ ns, and the time-frequency hopping code given in [6] Table 15, selecting one out of three frequency bands at a time. With this, the amplitude scaling factor for the OFDM signal becomes

$$\alpha = \sqrt{\frac{D_a \Delta_f T_{\text{SYM}}\, 3}{(T_{\text{SYM}} - T_{\text{GI}})\, 0.5\ \text{W}}} = 1.384 \cdot 10^{-3}$$

and the data rate is chosen to 110 Mb/s.

3.2.2 White-Noise Signal

We consider a reference scheme under the hypothesis that a pulsed signal with PRF R_p is modulated such that it appears as like white Gaussian noise with two-sided PSD $N_0/2$ that increases linearly with R_p, such that $N_0/2 = R_p E^t_{s,p}/2$, correspondingly, its average PSD is expressed by

$$D_a = R_p E^t_{s,p}. \tag{4}$$

Again, the ESD $E^t_{s,p} = 10^{-5}$ nWs/MHz, resulting for $R_p = 10$ MHz in a PSD $D_a = 100$ nW/MHz $\equiv -40$ dBm/MHz.

4 Average Power Measurement

4.1 Periodic Stream of Pulses

We make an approximative analysis of the measured average power P_a^m for the two PRF regions, $R_p < B_{af}$, and $R_p \geq B_{af}$. The Fourier transform of the signal $s(t)$ is given by

$$S(f) = \sqrt{\frac{E_{s,p}^t}{2}} R_p \sum_{k=-\infty}^{\infty} \delta(f - kR_p),$$

and the Fourier transform of the Gaussian resolution filter output becomes

$$Y(f) = \sqrt{\frac{E_{s,p}^t}{2}} R_p \sum_{k=-\infty}^{\infty} F(f - kR_p). \tag{5}$$

For $R_p \geq B_{af}$, we assume for simplicity that only a single spectral line of $S(f)$ can pass the bandpass resolution filter, consequently the sums in (5) do not overlap along the frequency axis; thus, the power spectrum becomes

$$|Y(f)|^2 = \frac{E_{s,p}^t R_p^2}{2} \sum_{k=-\infty}^{\infty} |F(f - kR_p)|^2, \quad R_p \geq B_{af}. \tag{6}$$

With this, the power at the resolution filter's output depends on its center frequency f_0, which according to [1] must be chosen such that the power at the filter output assumes its maximum value, which is $P_a^m = E_{s,p}^t R_p^2$, as can be observed from the two-sided power spectrum in (6) with $|F(f_0)|^2 = 1$ (Fig. 3).

For $R_p < B_{af}$, we must take into account the effect of the finite measurement duration $T = 1$ ms. The number of pulses whose energy is captured during this period varies between $\lfloor TR_p \rfloor$ and $\lceil TR_p \rceil$, depending on the time delay between the beginning of the measurement interval and the first captured pulse. For $R_p < B_{af}$, we assume for simplicity that the pulses at the filter output do not overlap along the time axis, hence the average power is approximated by the product of the energy per filtered pulse, $1.064\, E_{s,p}^t B_{af}$, and the number of captured pulses divided by the duration T, i.e., $1.064\, E_{s,p}^t B_{af} \frac{\lfloor TR_p \rfloor}{T} \leq P_a^m \leq 1.064\, E_{s,p}^t B_{af} \frac{\lceil TR_p \rceil}{T}$. The factor 1.064 stems from the equivalent noise bandwidth which is $1.064\, B_{af}$ or, equivalently, the impulse response energy of the Gaussian resolution filter.

PRFs lower than 10 KHz are unlikely to be used by UWB systems, therefore, in this work we follow the approach in [2] and [3] and restrict the analysis to PRFs higher than 10 KHz, see also Fig. 1 or Appendix E in [1]. For $R_p \geq 10$ KHz we approximate $\lfloor TR_p \rfloor \approx \lceil TR_p \rceil \approx TR_p$; with this and (6) the measured average power yields

$$P_a^m = \begin{cases} 1.064\, E_{s,p}^t B_{af} R_p, & \text{for } 10 \text{ KHz} \leq R_p < 1.064 B_{af}, \\ E_{s,p}^t R_p^2, & \text{for } 1.064\, B_{af} \leq R_p. \end{cases} \tag{7}$$

Although the above approximations are loose when R_p is approximately 10 KHz or B_{af}, this analytical consideration helps to explain the mechanisms that determine the average power of a periodic stream of pulses. The transition PRF, $R_p = 1.064 B_{af}$, was chosen to obtain a steady transition between the two functions in (7). An evaluation of (7) is depicted in Fig. 4(a), where it is labelled *theoretical: non-dithered.*

The simulated (measured) values for the average power of a periodic stream of pulses are also shown in Fig. 4(a), showing good agreement with the theoretical results. Note that the center frequency of the resolution filter is $f_0 = 528$ MHz and the set of PRFs at which the average power is evaluated are chosen such that one of the spectral lines of the signal $y(t)$ coincides exactly with f_0.

4.2 Binary Antipodal Modulated Stream of Pulses

The simulated (measured) values for the average power of this signal is depicted in Fig. 4(b); P_a^m is a function of the PRF increasing approximately linear with 10 dB per decade. When the signal $s(t)$ is white noise, the average power is exactly described by a linear function of the PRF, see Subsection 4.7. Hence, from an average power point-of-view, the spectrum of a 2PAM stream of pulses is approximately white. With the average power measurement setup described in Section 2, the UWB signal is observed for the duration of 1 ms. This is enough observation time to make the corresponding short-time spectrum sufficiently flat such that from the average power point-of-view, the signal $s(t)$ appears as white noise.

4.3 Time-Hopped Stream of Pulses

The simulated (measured) values for the average power of this signal is depicted in Fig 4(c). The average power for high PRFs oscillates between the average power of non-dithered and dithered signals. Therefore, from an average power point-of-view, a 2PPM stream of pulses cannot be considered white. To achieve better whitening of the signal, further dithering can be introduced by increasing the modulation order.

4.4 Combined Binary Antipodal and Time-Hopped Stream of Pulses

The simulated (measured) average power is depicted in Fig 4(d). The average power for this modulation scheme shows the same dependency on the PRF as the average power of a binary-antipodal modulated signal (Fig. 4(b)). It can by shown analytically, that a PPM modulated signal with arbitrary modulation order and randomly chosen pulse polarity, i.e., with overlayed 2PAM, has a white power spectrum [7]. Moreover, our result shows that not only the power spectrum of this type of signals is flat, but also the short-time power spectrum (for an observation

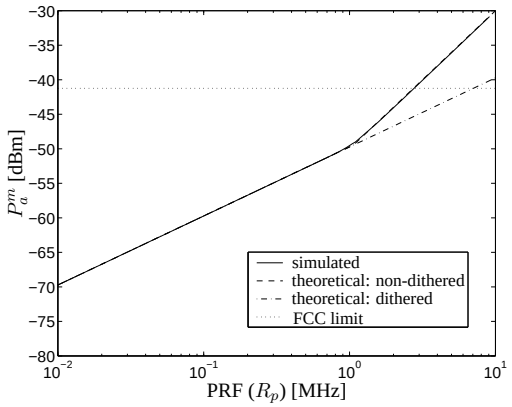

(a) Periodic stream of pulses (non-dithered).

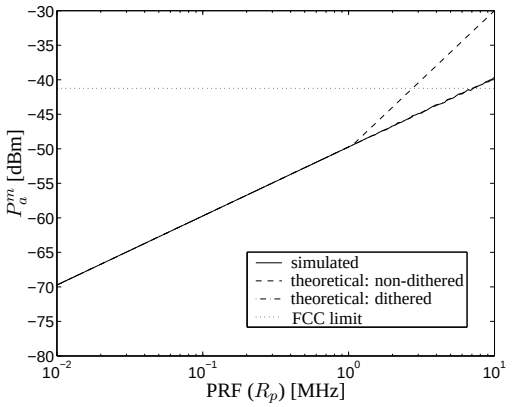

(b) Binary antipodal modulated stream of pulses (2PAM).

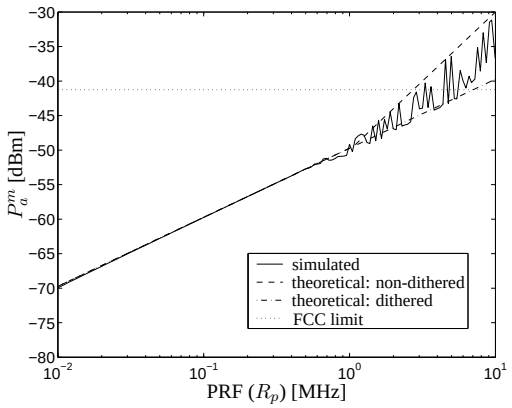

(c) Time-hopped stream of pulses (2PPM).

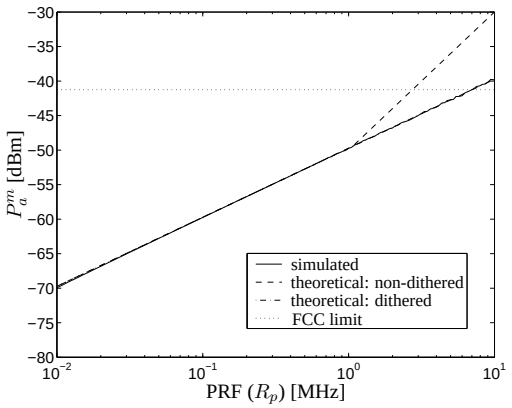

(d) Time-hopped and binary antipodal modulated stream of pulses (combined 2PPM/2PAM).

Figure 4: Simulated (measured) average power as a function of PRF and for different modulation schemes; the ESD of the transmitted pulses is $E_{s,p}^t = 10^{-5}$ nWs/MHz, correspondingly, for $R_p = 10$ MHz the PSD is $D_a = 100$ nW/MHz$\equiv -40$ dBm/MHz. The bandwidth of the resolution filter used for the measurement is $B_{af} = 1$ MHz; the curves labelled *theoretical: non-dithered* are only an approximation if the PRF, R_p, is close to B_{af}. The curves labelled *theoretical:dithered* correspond to white Gaussian white signals (see Subsection 4.7).

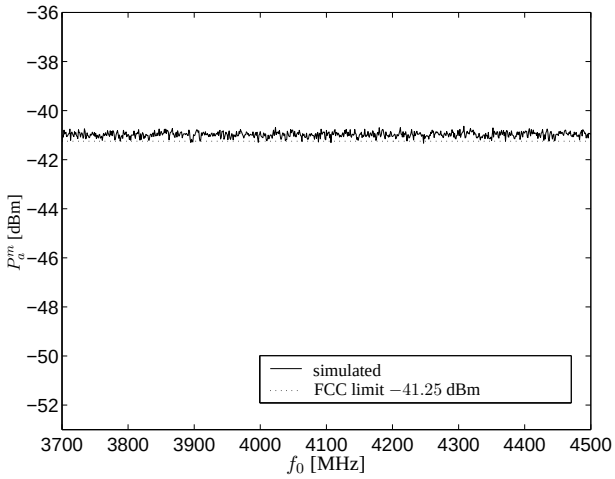

Figure 5: Average power of DSSS (or DS-UWB) signal emitte over 6 parallel channels, each supporting a data rate of 110 Mb/s.

duration of 1 ms). A similar result is documented in [8], where UWB signals filtered with the bandwidth of a 3G receiver are classified as white Gaussian noise within this filter bandwidth.

4.5 Direct-Sequence Spread-Spectrum

The simulated (measured) average power for six parallel DSSS (or DS-UWB) channels, each supporting a data rate of 110 Mb/s, is shown in Fig. 5. We observe that the average power level varies slightly as a function of the resolution filter's center frequency f_0. Hence, the PSD of this signal is not completely constant, i.e., the considered DSSS signal is only approximately white, although to a high degree. The power level averaged over f_0 corresponds approximately to the equivalent NBW, $1.064\ B_{af}$, of the resolution filter, specified in Subsection 2.1, times the signal's PSD, $D_a = -41.25$ dBm/MHz; this is because the spectrum of the considered signal is continuous. A spectrum analyzer used in practice, might have a resolution filter with a different equivalent NBW (B_{NBW}); as a consequence, depending on the spectrum analyzer's resolution filter, the current FCC limit of $D_a \equiv -41.25$ dBm/MHz should be scaled by the factor (B_{af}/B_{NBW}) to determine the transmitter's maximum average PSD.

If only one of the six available channels is transmitting with a data rate of 110 Mb/s, the DSSS signal is described by the binary antipodal modulated signal defined in Subsection 3.1, with the PRF set to one of the values from the set $\{1300/6, 1313/6, 1326/6, 1339/6, 1352/6, 1365/6\}$ MHz.

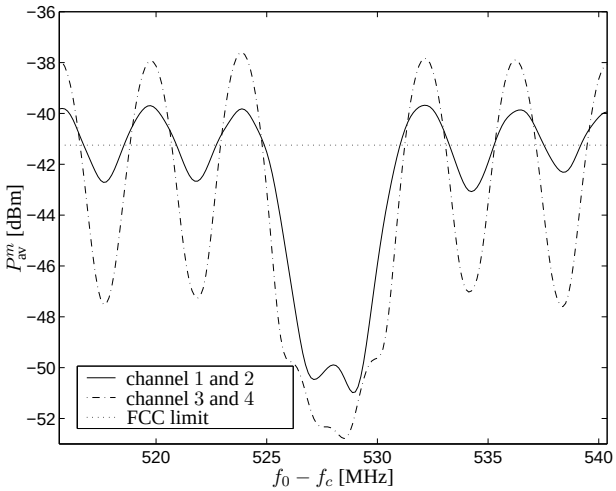

Figure 6: Measured average power as a function of the difference between the center frequency (f_0) of the resolution filter and the center frequency (f_c) of OFDM Band 1.

4.6 Multiband-OFDM Signal

The PSD of an UWB signal is flat (white) in the ideal case. Generally, however, the PSD changes with frequency, e.g., the signal's measured average power, P_a^m, depends on the center frequency, f_0, of the resolution filter; this is the case for the multiband-OFDM signal as can be seen from Fig. 6. This effect, however, is stronger if Channels 3 and 4 are chosen, while it is weaker for channels 1 and 2; this difference occurs because the frequency-hopping sequence depends on the channel number. For Channels 1 and 2 the signal frequency changes after transmission of every OFDM symbol, while for Channels 3 and 4 two successive OFDM symbols are transmitted with the same frequency. Furthermore, for the considered data rate of 110 Mb/s, the two OFDM symbols in succession contain the same information. Therefore, we conclude that the duration of a OFDM symbol is virtually doubled if Channel 3 or 4 is used; this reduces the actual bandwidth of the subbands and therefore causes a higher ripple in the power spectrum. Figure 6 also depicts the FCC limit of the average PSD, which coincides with $D_a \equiv -41.25$ dBm/MHz of the emitted OFDM signal, see Subsection 3.2. To stay within the FCC average power limit as measured by a spectrum analyzer, an average emitted PSD of $D_a \approx -42.65$ dBm/MHz is allowed on Channel 1 or 2 and $D_a \approx -44.45$ dBm/MHz on Channel 3 or 4. The result in Fig. 6 for Channel 1 and 2 is also confirmed in [9]. The power spectrum of OFDM signals is computed analytically in [10] for an observation window of infinite durtion.

4.7 White-Noise Signal

For white noise-like signals the measured average power is given by the simple expression

$$P_a^m = 1.064\, B_{af} R_p E_{s,p}^t \tag{8}$$

and the corresponding curve is depicted in Fig. 4 and denoted *theoretical: dithered.* The factor 1.064 stems form the equivalent noise bandwidth, $N_{\text{NBW}}\ 1.064\, B_{af}$, of the Gaussian resolution filter, see Subsection 2.1 . The same average power is obtained for 2PAM, and combined 2PAM/2PPM signals, see Fig. 4(b) and 4(d) respectively.

5 Peak Power Measurement

The peak power of dithered and non-dithered signals can be determined analytically on the basis of the average power of dithered and non-dithered signals, and the PAPR given in Fig. 1. An analytical description of the PAPR can be found in Appendix D of [3][5], which for *non-dithered* signals is summarized by

$$\frac{P_p^m}{P_a^m} = \begin{cases} \frac{B_{pf}^2}{0.45^2 B_{af} R_p}, & \text{for } R_p \le B_{af}, \\ \left(\frac{B_{pf}}{0.45 R_p}\right)^2, & \text{for } B_{af} < R_p \le B_{pf}/0.45, \\ 1, & \text{for } B_{pf}/0.45 < R_p, \end{cases} \tag{9}$$

and for *dithered* signals by

$$\frac{P_p^m}{P_a^m} = \begin{cases} 5\,\frac{B_{pf}^2}{B_{af} R_p}, & \text{for } R_p \le \frac{1}{2} B_{pf}, \\ 10\,\frac{B_{pf}}{B_{af}}, & \text{for } \frac{1}{2} B_{pf} < R_p. \end{cases} \tag{10}$$

The measured peak power is computed by multiplying the PAPR in (9) and (10) with P_a^m given by (7) and (8) for non-dithered and dithered signals, respectively. Thus, the resulting peak power for *non-dithered* signals is

$$P_p^m = \begin{cases} 5.254\, E_{s,p}^t B_{pf}^2, & \text{for } R_p < B_{af}, \\ 5.254\, \frac{E_{s,p}^t B_{pf}^2 B_{af}}{R_p}, & \text{for } B_{af} < R_p \le 1.064\, B_{af}, \\ 4.938 E_{s,p}^t B_{pf}^2, & \text{for } 1.064\, B_{af} < R_p \le B_{pf}/0.45, \\ R_p^2 E_{s,p}^t, & \text{for } B_{pf}/0.45 < R_p, \end{cases} \tag{11}$$

[5] In this document the PAPR is denoted by the term *bandwidth correction factor peak* (BWCF_p).

and the resulting peak power for *dithered* is

$$P_p^m = \begin{cases} 5.320\, E_{s,p}^t B_{pf}^2, & \text{for } R_p < B_{pf}/2, \\ 10.64\, E_{s,p}^t B_{pf} R_p, & \text{for } B_{pf}/2 \le R_p. \end{cases} \tag{12}$$

The numerical values of these expressions are displayed in Fig. 1 for two resolution bandwidths, $B_{pf} = 1$ MHz and 50 MHz, and labelled *NTIA equivalent*. Fig. 1 also shows the peak power limit, which is 1 mW for $B_{pf} = 50$ MHz and $(B_{pf}/50\text{ MHz})^2$ mW for 1 MHz $\le B_{pf} \le 50$ MHz. The results can be verified by comparing Fig. 1 with Fig. 1 and Fig. 4.

To verify these results, we directly derive approximate expressions for the measured peak power of non-dithered signals. If the PRF $R_p < B_{pf}$, we assume for simplicity, that the pulses at the resolution filter output do not overlap. Thus, for the non-dithered pulse sequence specified in (2), the measured peak power is

$$\begin{aligned} P_p^m &= \frac{1}{2}\left(\sqrt{\frac{E_{s,p}^t}{2}} f(0)\right)^2 \\ &= \frac{\pi E_{s,p}^t B_{pf}^2}{2\ln(2)} \\ &= 2.266\, E_{s,p}^t B_{pf}^2, \end{aligned} \tag{13}$$

where $f(0)$ is the peak value of the resolution filter's impulse response given in (1). If the PRF $R_p > B_{pf}$, the pulses at the resolution filter output will overlap; if furthermore R_p is an integer fraction of f_0, i.e., $f_0 = nR_p$, $n \in \mathbb{N}$, than the pulse amplitudes will add exclusively in a constructive manner. This observation is the key to derive the upper bound on P_a^m, i.e.,

$$P_a^{m,u} = \frac{1}{2}\left[\sqrt{\frac{E_{s,p}^t}{2}} \sum_{n=-\infty}^{\infty} f\left(\frac{n}{R_p}\right)\right]^2.$$

For $R_p \gg B_{pf}$ a simple approximation of this expression can be found which becomes exact for $\lim R_p \to \infty$, i.e.,

$$\begin{aligned} \lim_{R_p\to\infty} P_a^{m,u} &= \frac{1}{2}\left[\sqrt{\frac{E_{s,p}^t}{2}} R_p \int_{\infty}^{\infty} \frac{f(t)}{\cos(2\pi f_0 t)} dt)\right]^2 \\ &= \frac{E_{s,p}^t R_p^2}{4}\left(B_{pf}\sqrt{\frac{2\pi}{\ln(2)}} \int_{-\infty}^{\infty} e^{-\frac{(\pi B_{pf} t)^2}{2\ln(2)}} dt\right)^2 \\ &= E_{s,p}^t R_p^2. \end{aligned}$$

Dividing $f(t)$ by $\cos(\cdot)$ corresponds to the assumption of exclusively constructive pulse addition (see (1)). Combining the results for both R_p regions discussed above yields the upper bound on

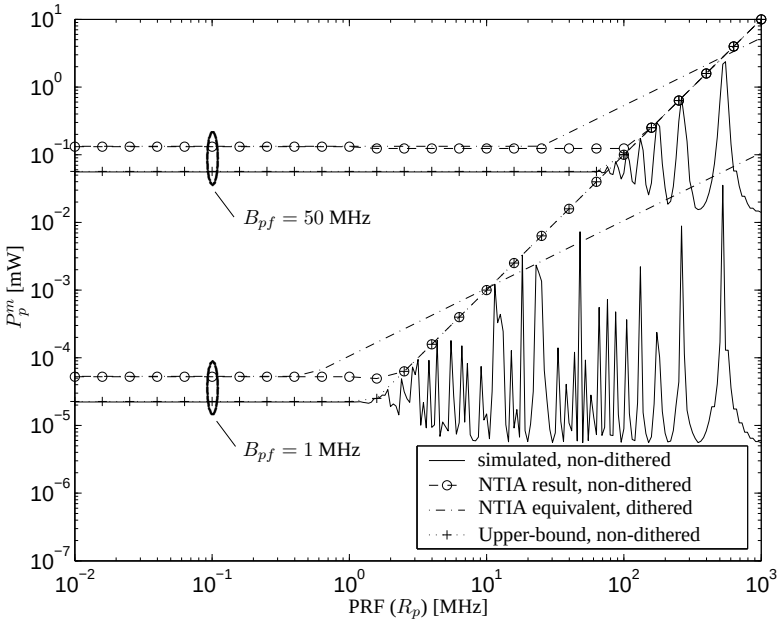

Figure 7: Peak power functions (11), (12), and simulated peak power of periodic stream of pulses (*non-ditered*), for resolution bandwidths, B_{pf}, of 1 MHz and 50 MHz. Also shown is the upper bound (14) on P_a^m for *non-dithered* signals.

P_a^m of *non-dithered* signals:

$$P_a^{m,u} = \begin{cases} 2.266\, E_{s,p}^t B_{pf}^2, & \text{for } R_p < 1.505\, B_{pf}, \\ E_{s,p}^t R_p^2, & \text{for } 1.505\, B_{pf} \le R_p. \end{cases} \tag{14}$$

The transition PRF, $R_p = 1.505\, B_{pf}$, was chosen to obtain a steady transition of the peak power between the two functions in (14). The analytical result (14) is depicted in Fig. 7 together with simulation results, showing very good agreement.

Figure 7 also depicts the NTIA equivalent peak power for non-dithered signals given in (11), and for dithered signals given in (12), showing a deviation from the simulation results of approximately a factor of two for PRFs where $R_p < 1.505\, B_{pf}$ and a perfect match where $R_p > 2.266\, B_{pf}$. A possible reason for this mismatch is the resolution filter $F(f)$ in the spectrum analyzer used by the NTIA, which is likely not exactly Gaussian and/or not phase linear; there might be additional mismatches between real spectrum analyzers and our model (Fig. 2).

Note that the measured peak power depends not only on the bandwidth of the resolution filter, but on additional frequency- and phase spectrum details. To show this, we consider as an example the measured peak power when an ideal bandpass filter is used, instead of the Gaussian resolution filter, and when the measured signal is a single Dirac delta pulse with one-sided ESD

$E^t_{s,p}$; the bandwidth of the filter is B_{pf}, the center frequency is f_0 and the gain in the passband is unity and zero outside. As shown in Appendix A, the corresponding impulse response is $h(t) = 2B_{pf}\cos(2\pi f_0 t)\sin(\pi B_{pf} t)/(\pi B_{pf} t)$; with this, the peak power at the filter output yields

$$P_p^m = \frac{1}{2}\left[\sqrt{\frac{E^t_{s,p}}{2}}h(0)\right]^2 = E^t_{s,p}B^2_{pf}.$$

This peak power is less than half the peak power of the Gaussian filter's impulse response, see (13). This is because the impulse response of the Gaussian bandpass filter is more concentrated in time as the corresponding frequency response is more spread in the frequency domain. Note that the impulse response of the Gaussian bandpass filter has 1.064 times the energy of the impulse response of the ideal bandpass filter.

5.1 Periodic Stream of Pulses

The simulated (measured) peak power for this type of non-dithered signal is shown in Fig. 8(a) as a function of the PRF. For PRF's lower than about $1.5\,B_{pf}$ the peak power does not depend on the PRF and for PRF's higher than about $1.5\,B_{pf}$, the peak power shows spikes whose magnitude increases with 20 dB/decade, thus perfectly confirming the analytically found upper bound given in (14). The spikes of the peak power curve for $B_{pf} = 1$ MHz do not reach this upper bound for PRFs where $R_p > 20$ MHz; this is because the peak power equals the upper bound (14) only for certain PRFs, which for this example are not in the set of PRFs used in the simulation (see the derivation of (14)). Note that the PRFs at which spikes occur depend on the center frequency, f_0, of the resolution filter. For PRFs $R_p < 1.5\,B_{pf}$ the simulated peak power value is about a factor of two below the NTIA equivalent value, as already mentioned above; a possible reason for this deviation is the mismatch between our modeling of the measurement systems (Fig. 2) and the real instruments employed by the NTIA.

Fig. 8(a) shows also the FCC's peak power limit of $(B_{pf}/50\,\text{MHz})^2$ mW for $B_{pf} = 1$ MHz and 50 MHz. Under the current assumptions on the value of $E^t_{s,p}$ (10^{-5} nW/MHz), for $B_{pf} = 50$ MHz this limit is exceeded by the NTIA equivalent peak power for $R_p > 200$ MHz, whereas for $B_{pf} = 1$ MHz it is already exceeded for $R_p > 6$ MHz. We conclude that the FCC emission limits [1] are gradually more stringent the *lower* the resolution bandwidth used for the peak power measurement is. The same effect can be observed for all signal types discussed in the sequel. As an additional example, the NTIA equivalent peak power for dithered signals depicted in Fig. 8(c) indicates a maximum sustainable PRF of about 200 MHz for $B_{pf} = 50$ MHz but only about 4 MHz when $B_{pf} = 1$ MHz. The reason for this is the FCC's choice of the peak power emission limit of $(B_{pf}/50\,\text{MHz})^2$ mW; the FCC is aware of the fact that this choice is rather conservative [1]. Note that the total transmitted signal power $E^t_{s,p}R_p$ linearly increases

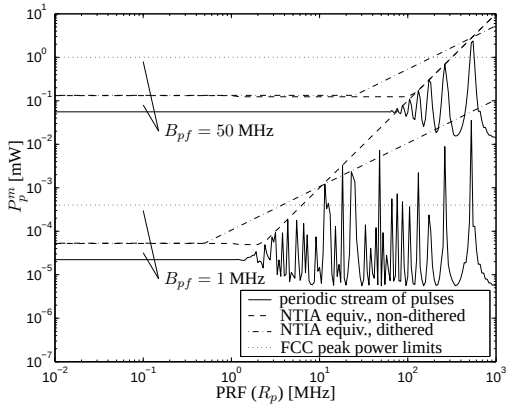

(a) Periodic stream of pulses (Non-dithered signal).

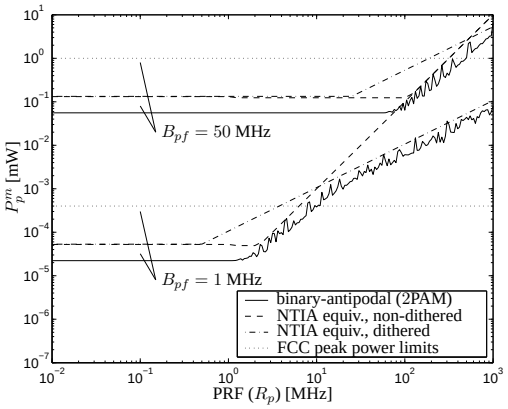

(b) Binary antipodal modulated stream of pulses (2PAM).

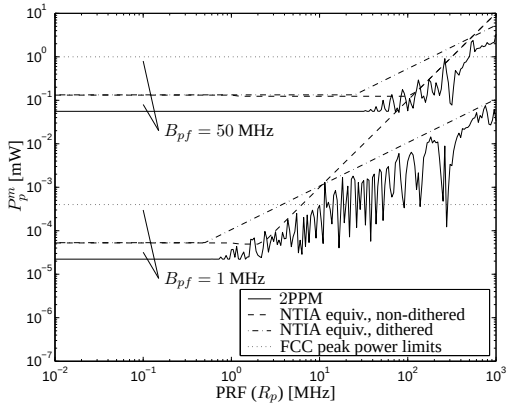

(c) Time-hopped stream of pulses (2PPM).

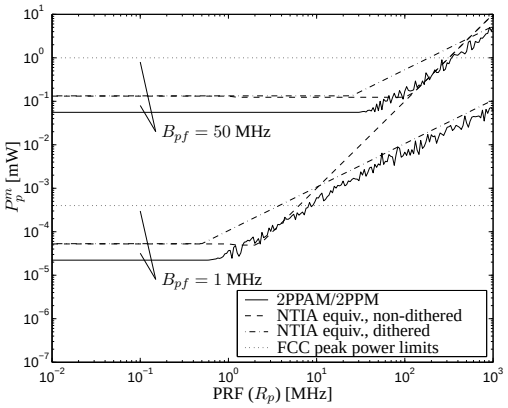

(d) Binary antipodal time-hopped stream of pulses (combined 2PAM-2PPM).

Figure 8: Simulated peak power as a function of PRF for different modulation schemes, the ESD of the transmitted pulses is $E_{s,p}^t = 10^{-5}$ nWs/MHz.

with the PRF, R_p, see Subsection 3.1.

5.2 Binary Antipodal Modulated Stream of Pulses

The peak power of a binary antipodal modulated (2PAM) stream of pulses is depicted in Fig. 8(b). We observe that for a PRF above about $10\,B_{pf}$, the spikes of the simulated peak power meet the NTIA equivalent peak power for dithered signals given by (12). For PRFs in the interval $[1.505\,B_{pf},\ 10\,B_{pf}]$ the peak power spikes are limited by the NTIA equivalent peak power curve for non-dithered signals, which in this PRF region is below the curve of dithered signals. For PRFs lower than about $1.505\,B_{pf}$, the peak power is lower than the NTIA equivalent peak power for both dithered and non-dithered signals; a possible reason for this deviation is the mismatch between our modeling (Fig. 2) and real spectrum analyzers, as explained above.

Note that interference of overlapping pulses results in an increased peak power level if the interference is constructive. The interference of adjacent pulses is determined by the modulating symbol sequence and the PRF (see (3)), hence the maximum peak power depends on the modulating symbol sequence and on the PRF. Symbol sequences occur with certain probabilities, *hence the peak power observed in a finite time interval is a random variable*. This implies that the observation interval must be long enough to ensure with a certain probability that the maximum possible peak power can be observed; this holds for all signals whose modulation involves random variables. In this work the signal observation time for peak power simulation was set to 0.1 ms (See Subsection 2.4).

5.3 Time-Hopped Stream of Pulses

Fig. 8(c) shows the simulated peak power for a 2PPM signal as a function of the PRF, with spikes of similar magnitude as shown in Fig. 8(b) for 2PAM signals. However, the peak power of the 2PPM signal begins to rise at a lower PRF of about $R_p = 0.5B_{pf}$. This is because dithered signals are defined as randomly time-hopped signals (see [3]), which cause pulses at the output of the resolution filter to overlap for PRF's of only about half the filter bandwidth B_{pf}, while 2PAM signals cause pulses to overlap only if $R_p \gtrapprox B_{pf}$.

5.4 Combined Binary-Antipodal and Time-Hopped Stream of Pulses

When the two modulation schemes, 2PAM and 2PPM are combined, than the peak power characteristics are very similar to that of a 2PAM signal alone. However, for the reasons discussed above, the peak power of the 2PAM/2PPM signal begins to increase already with lower PRFs; this effect is also pointed out in [11]. An offset of up to 3 dB between the NTIA equivalent peak

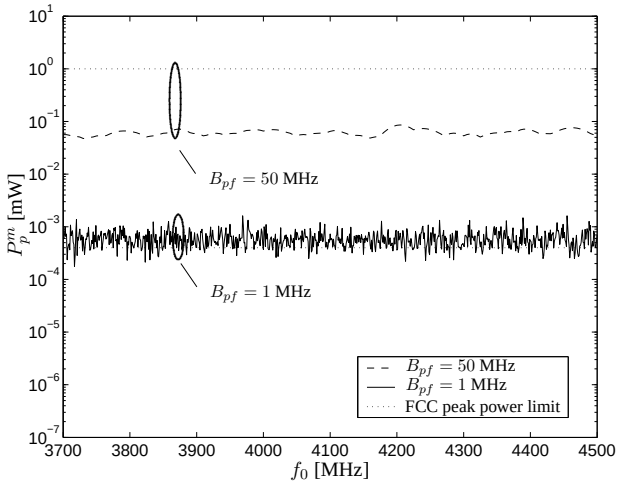

Figure 9: Peak power of DSSS (or DS-UWB) signal for 6 parallel channels, each with a data rate of 110 Mb/s and for $B_{pf} = 1$ MHz and 50 MHz.

power and the simulated (measured) peak power can be observed in all plots of Fig. 8 for PRFs where $R_p \lessapprox B_{pf}$ this point is also discussed in [11].

5.5 Direct-Sequence Spread-Spectrum

The peak power of the DSSS (or DS-UWB) signal consisting of six channels, where each supports a data rate of 110 Mb/s, is depicted in Fig. 9. The peak power varies over the center frequency, f_0, of the resolution filter; this is the same effect that can be observed for the average power shown in Fig. 5. The peak power measured with 50 MHz RBW is averaged over a larger bandwidth and thus smoother than the peak power measured with the 1 MHz RBW. Furthermore, for a transmitted PSD of $D_a = -41.25$ dBm/MHz and for 50 MHz RBW, the peak power is far below the peak power limit of 1 mW; however, for a 1 MHz RBW the peak power limit of $(1\text{ MHz}/50\text{ MHz})^2$ mW is exceeded. We conclude that the scaling factor $(1\text{ MHz}/50\text{ MHz})^2$ proposed by the FCC is too conservative for the considered DSSS.

The maximum observed peak power for a 50 MHz and a 1 MHz RBW is $1.622\,10^{-3}$ mW and $8.588\,10^{-2}$ mW, respectively; these values will be used in Subsection 7.1 to formulate a peak power constraint that is independent of the RBW indicated by the value of B_{pf}. If only one of the six available channels is transmitting with a data rate of 110 Mb/s, the DSSS signal is described by the 2PAM signal defined in Subsection 3.1, with the PRF set to one of the values from the set $\{1300/6, 1313/6, 1326/6, 1339/6, 1352/6, 1365/6\}$ MHz.

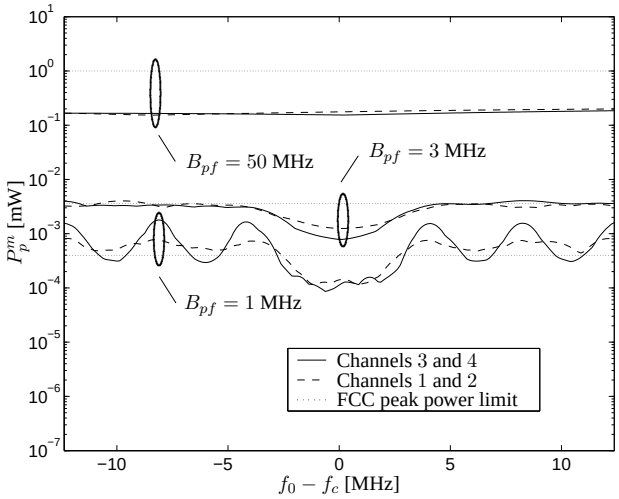

Figure 10: Peak power of multiband-OFDM signals for 1 MHz 3 MHz and 50 MHz RBW.

5.6 Multiband-OFDM Signal

The simulated (measured) peak power for multiband-OFDM signals is shown in Fig. 10. For a resolution filter bandwidth $B_{pf} = 50$ MHz, the peak power shows almost no sensitivity to the center frequency, f_0, of the resolution filter; however, for $B_{pf} = 1$ MHz, the spectrum of the OFDM signal is better resolved such that the peak power depends on f_0. For the reasons mentioned in Subsection 4.6, this dependency on f_0 is larger if Channel 3 or 4 is selected. Note that the FCC's peak power limit is not critical for $B_{pf} = 50$ MHz and 3 MHz, while it is exceeded for $B_{pf} = 1$ MHz; this indicates that the scaling factor $(B_{pf}/50 \text{ MHz})^2$ is for multiband-OFDM signals rather conservative.

5.7 White Gaussian Noise

We assume an UWB signal that is white Gaussian noise with one-sided PSD

$$D_a = R_p E_{s,p}^t,$$

where $E_{s,p}^t$ is defined in Section 3. The power of the noise signal, filtered with the Gaussian bandpass filter with bandwidth B_{pf}, is $D_a B_{pf}$. Hence, the variance of the bandpass filtered noise signal is $\sigma^2 = N_0 B_f$. The peak power depends on the probability density function (PDF) of the noise signal and is thus infinite for a Gaussian PDF. However, it is possible to specify a peak power level $P_p(x)$ that is exceeded with probability x, see Appendix B. In Fig. 11 the peak power of such a white Gaussian noise signal is shown as a function of the PRF. For comparison the NTIA equivalent peak power for dithered signals, (11) is also shown. From Fig. 11 we

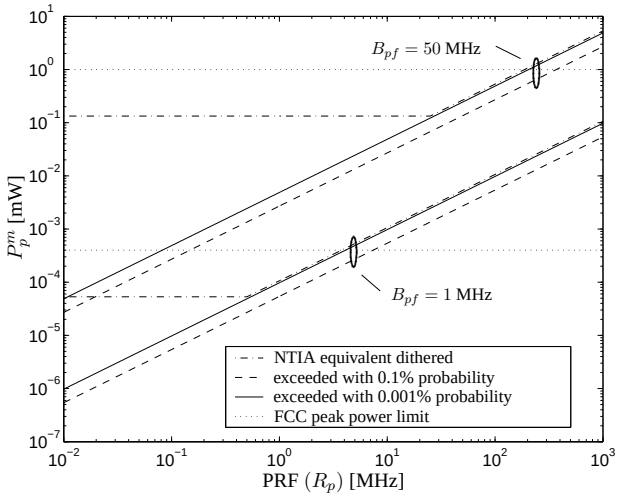

Figure 11: Peak power of white noise-like signals with Gaussian amplitude distribution and pulse ESD $E_{s,p}^t = 10^{-5}$ nWs/MHz, compared to the peak power of a dithered signal with the same pulse ESD, i.e., with the same average power.

conclude that white Gaussian noise-like signals produce similar peak power levels as pulsed UWB signals for high PRFs, i.e., when the pulses of the resolution filter output overlap; for low PRFs the noise signal produces a much lower peak power value.

5.8 Summary (Peak Power)

The measurement or resolution bandwidth, $B_{pf} = 50$ MHz was proposed by the FCC because this is considered to be the widest *expected* bandwidth of a practical victim receiver, thus resulting in the highest observable interference power caused by a UWB signal. However, the resolution bandwidth of common spectrum analyzers is lower than 50 MHz, therefore, the FCC proposed to perform the peak power measurement with a resolution bandwidth of only 3 MHz. According to this FCC proposal, the corresponding result measured with some B_{pf} value between 1 MHz and 50 MHz must be divided by the scaling factor $(B_{pf}/50 \text{ MHz})^2$ to compute the equivalent peak power that would be measured with a 50 MHz resolution bandwidth.

We observe that the scaling factor $(B_{pf}/50 \text{ MHz})^2$ is fair for pulsed signals with PRF $R_p < B_{pf}/2$. However, for pulsed signals with higher PRFs, multiband-OFDM signals, and white Gaussian noise signals, the peak power scaling factor $(B_{pf}/50 \text{ MHz})^2$ is too conservative. This leads to the effect that the maximum allowed emitted PSD is decreased when the peak power is measured with a lower resolution filter bandwidth. In addition, the use of a measurement bandwidth smaller than 50 MHz leads to a reduction of the maximum allowed PRF; the same issue is discussed in [12].

6 Maximum Allowed Transmitted Pulse ESD and PSD

We now determine the ESD per transmitted pulse, $E^t_{s,p}$, and the PSD, $D_a E^t_{s,p} R_p$ of UWB signals, such that both the FCC's peak- and average power constraints are satisfied but fully exploited. From [1], the average power constraint is

$$P^m_a \leq \hat{P}^m_a = 75 \text{ nW} \equiv -41.25 \text{ dBm}, \tag{15}$$

and the peak power constraint is

$$P^m_p \leq \hat{P}^m_p = \left(\frac{B_{pf}}{50 \text{ MHz}} \right)^2 \text{ mW}, \tag{16}$$

i.e., we have

$$P^m_p \leq \begin{cases} 1 \text{ mW}, & \text{for } B_{pf} = 50 \text{ MHz}, \\ 4 \cdot 10^{-4} \text{ mW}, & \text{for } B_{pf} = 1 \text{ MHz}. \end{cases}$$

For simplicity we restrict the analysis of the emission limits to non-dithered and dithered signals. The peak power and average power values of these signal types are close to those of the pulsed modulation schemes considered in Sections 4 and 5; thus, the corresponding emission limits can also be assessed for these modulation schemes.

The peak and average power for non-dithered and dithered signals have been determined in multiple ways in the previous sections. We chose those methods, which correspond best with the NTIA's results that eventually will be used for testing a device. Therefore, we use the peak power expressions (11) and (12) which have been determined indirectly by using the analytical average power results of Section 4 and the PAPR documented in [3]. These PAPRs are based on real measurements and simulation results reported in [2], therefore, we expect them to agree well with real measurement results. While peak power measurements are very sensitive to actual conditions, even the phase spectrum of the resolution filter impacts the measurement results, average power measurements are less sensitive to the chosen measurement equipment. Therefore, we are confident that the average power determined in Section 4 by analysis and simulation is very close to actual measurement results; our results also support the validity of the peak power expressions (11) and (12). In fact, for the present purpose, we can simplify (11) by combining the first three functions:

$$P^m_p = \begin{cases} 5.254 \, E^t_{s,p} B^2_f, & \text{for } R_p < 2.292 \, B_{pf}, \\ R^2_p E^t_{s,p}, & \text{for } 2.292 \, B_{pf} \leq R_p. \end{cases} \tag{17}$$

6.1 Non-Dithered Signals

The maximum allowed ESD, $\hat{E}^t_{s,p}$, based on the average power constraint and the peak power constraint is obtained by solving (7) and (17) for $E^t_{s,p}$ and substituting $E^t_{s,p}$, P^m_a, and P^m_p by

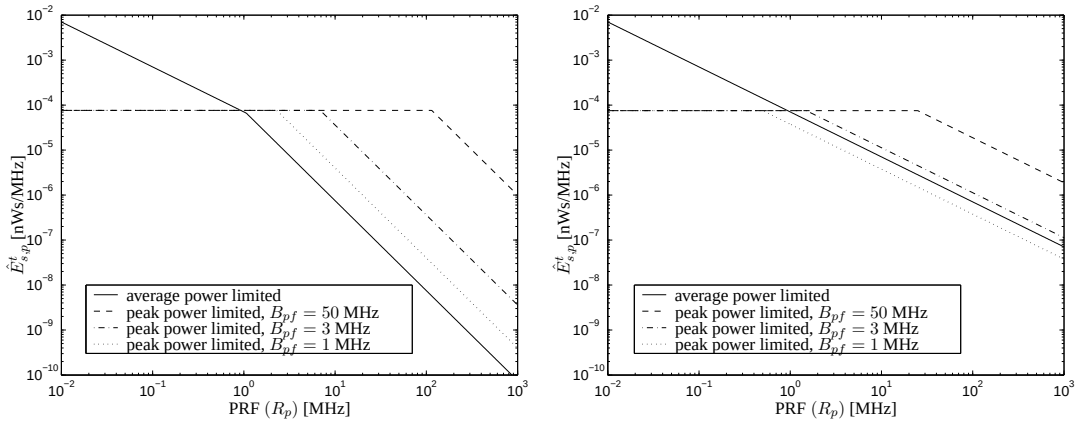

(a) Non-dithered signals

(b) Dithered signals

Figure 12: Maximum allowed ESD per emitted pulse satisfying the average or peak power constraint for non-dithered and dithered signals.

$\hat{E}^t_{s,p}$, $\hat{P}^m_a$ and $\hat{P}^m_p$, respectively. For the average power constraint we then obtain

$$E^t_{s,p} \le \hat{E}^t_{s,p} = \begin{cases} 0.9398\,\frac{\hat{P}^m_a}{B_{af} R_p}, & \text{for } 10 \text{ KHz} \le R_p < 1.064\,B_{af}, \\ \frac{\hat{P}^m_a}{R_p^2}, & \text{for } 1.064\,B_{af} \le R_p, \end{cases} \tag{18}$$

and the peak power constraint becomes

$$E^t_{s,p} \le \hat{E}^t_{s,p} = \begin{cases} 0.1903\,\frac{\hat{P}^m_p}{B_{pf}^2}, & \text{for } 10 \text{ KHz} \le R_p < 2.292\,B_{pf}, \\ \frac{\hat{P}^m_p}{R_p^2}, & \text{for } 2.292\,B_{pf} \le R_p. \end{cases} \tag{19}$$

$\hat{E}^t_{s,p}$ is shown in Fig. 12(a) as a function of the PRF, R_p. The corresponding constraint on the signal's PSD is obtained by multiplying the expressions in (18) and (19) with R_p; the result is shown in in Fig. 13(a). We conclude that for non-dithered signals, the maximum signal-power can be achieved for a PRF of $R_p \approx 1$ MHz; the average and the peak power constraints are both active for this PRF. The signal's PSD is limited by the peak power constraint for lower PRFs and the average power constraint provides a limit at PFRs higher than $R_p \approx 1$ MHz.

6.2 Dithered Signals

In analogy to the previous subsection we solve (8) and (12) for $E^t_{s,p}$, and substitute $E^t_{s,p}$, P^m_a, and P^m_p by $\hat{E}^t_{s,p}$, $\hat{P}^m_a$, and $\hat{P}^m_p$, respectively. The resulting maximum allowed ESD, $\hat{E}^t_{s,p}$, based

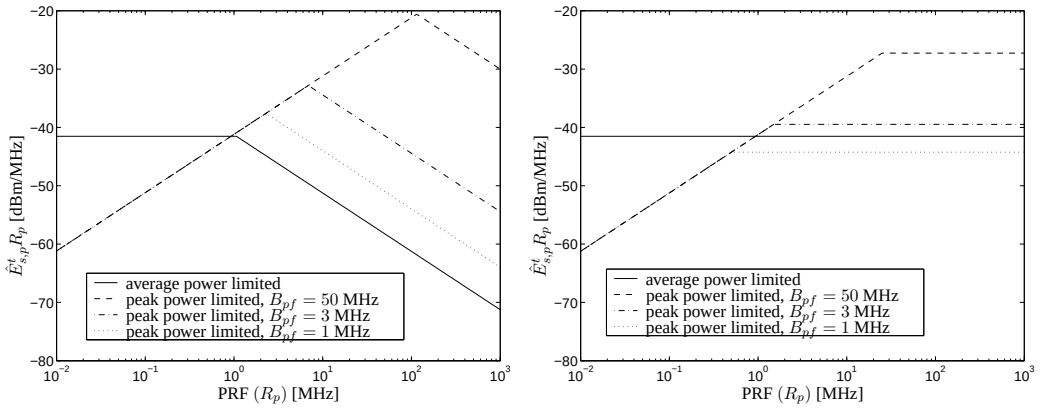

(a) Non-dithered signals

(b) Dithered signals

Figure 13: Maximum allowed PSD due to average power and peak power constraint, for non-dithered and dithered signals.

on the average power constraint becomes

$$E^t_{s,p} \leq \hat{E}^t_{s,p} = 0.9398 \, \frac{\hat{P}^m_a}{B_{af} R_p}, \tag{20}$$

and the peak power constraint yields the limit

$$E^t_{s,p} \leq \hat{E}^t_{s,p} = \begin{cases} 0.1880 \, \frac{\hat{P}^m_p}{B^2_{pf}}, & \text{for } 10 \text{ KHz} \leq R_p < \frac{1}{2} B_{pf}, \\ 0.09398 \, \frac{\hat{P}^m_p}{B_{pf} R_p}, & \text{for } \frac{1}{2} B_{pf} \leq R_p. \end{cases} \tag{21}$$

The dependency of $\hat{E}^t_{s,p}$ on the PRF, R_p is illustrated in Fig. 12(b). The corresponding value for the signal's PSD is obtained by multiplying the expressions in (20) and (21) with R_p; Fig. 13(b) shows the PSD's dependency on the PRF, R_p. When the peak power is measured with a resolution bandwidth $B_{pf} = 1$ MHz, then the maximum emitted power can be achieved for approximately $R_p > 0.5$ MHz; in the entire PRF region only the peak power constraint is active. For $B_{pf} = 1.875$ MHz and $R_p \geq B_{pf}/2$, the average power constraint and the peak power constraint are both active as can be derived from (16), (20) and (21). Thus, if the RBW, B_{pf}, used to measure the peak power is larger than 1.875 MHz, then the average power alone is active for PRFs $R_p > 1.875/2$ MHz $= 0.9375$ MHz. Thus, in this range and compared to the case where $B_{pf} = 1$ MHz, the maximum allowed emitted PSD increases by about 3 dB (see Fig. 13(b)). Therefore, if the RBW chosen to measure the peak power is exceeds 1.875 MHz (the FCC suggests the value $B_{pf} = 3$ MHz), then the maximum allowed emitted PSD remains the same for all RBWs up to 50 MHz, see Fig. 13(b).

Note that this holds for the current FCC average power limit of $\hat{P}_a^m = -41.25$ dBm and peak power limit of $\hat{P}_p^m = (B_{pf}/50\text{ MHz})^2$ mW; if, however, the ratio of the peak power limit to the average power limit, $\hat{P}_p^m/\hat{P}_a^m$, is decreased by more than about 2.5 dB (see Fig. 13(b)), then the RBW must be raised from 1.875 MHz above the value of 3 MHz to make the maximum allowed emitted PSD independent of the RBW. For this case, methods to measure the peak power are suggested in Section 7.

7 Suggestions for Peak Power Measurements

The scaling of the peak power limit $\hat{P}_p^m = (B_{pf}/50\text{ MHz})^2$ mW was introduced by the FCC, following a suggestion of the NTIA to enable peak power measurements with a RBW lower than 50 MHz. The reason was that spectrum analyzers with a RBW of 50 MHz are hardly available. This means, at least in principle, that a measurement result based on a RBW, e.g., when $B_{pf} = 3$ MHz, must be divided by the scaling factor $(B_{pf}/50\text{ MHz})^2$ to obtain the same result as if the RBW was $B_{pf} = 50$ MHz. However, the NTIA points out in [2] what we also found in Section 5:

> The exact scaling factor depends on the signal's modulation scheme and on the modulation parameters, e.g., the PRF (R_p) when pulsed modulation is applied. *The scaling factor $(B_{pf}/50MHz)^2$ is a lower bound for non-dithered pulse modulated signals with $R_p < 0.5\,B_{pf}$ and is too low for other modulation schemes.*

However, our results above show that, depending on the average- and peak power limits, this can result in a reduced maximal allowed peak power when the RBW is smaller than 50 MHz. There is no justification for such a disadvantage, as the maximal allowed power limit for a 50 MHz RBW has been chosen based on the assumption that no victim receiver would suffer harmful interference from transmitting UWB devices. Thus, we propose two alternative solutions to this problem: (a) the peak power of UWB devices should be truly measured with a 50 MHz resolution bandwidth, as it can be expected that most manufacturers of spectrum analyzer would react and offer analyzers with the required resolution bandwidth; (b) the RBW is variable within the range of $[1, 50]$ MHz and the required scaling factors (relative to the 1 mW peak power limit for $B_{pf} = 50$ MHz) must be determined for each modulation scheme and set of modulation parameters and for any chosen RBW within the range of $[1, 50]$ MHz. Both solutions have the advantage that the peak power limit can be fully exploited by all modulation schemes.

7.1 Scaling Factors

We define the scaling factor (SF) used in the proposed alternative (b) as the ratio of the peak power $P_p^m(B_{pf})$, measured with a RBW B_{pf}, to the peak power $P_p^m(50\text{ MHz})$, measured with

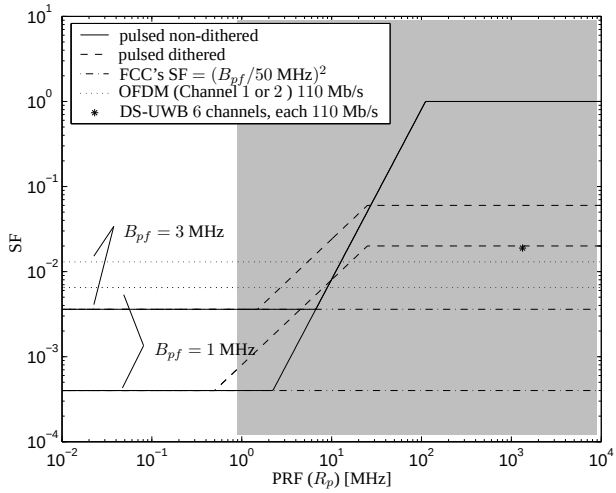

Figure 14: Scaling factors (SF) $\frac{P_p^m(B_{pf})}{P_p^m(50\ \text{MHz})}$ for $B_{pf} = 1$ MHz and 3 MHz for different modulation schemes and PRFs. The scaling factors for DS-UWB signals are only determined for $B_{pf} = 1$ MHz.

the reference RBW, $B_{pf} = 50$ MHz, i.e.,

$$\text{SF} = \frac{P_p^m(B_{pf})}{P_p^m(50\ \text{MHz})}. \tag{22}$$

In contrast, the SF proposed by the FCC is $(B_{pf}/50\ \text{MHz})^2$; in general, however, the SF depends on all parameters of the applied modulation scheme. As an example we consider SFs for non-dithered pulsed, DSSS (or DS-UWB), and multiband-OFDM signals.

For non-dithered signals, the reference peak power $P_p^m(50\ \text{MHz})$ is depicted in Fig 4(a), the peak power oscillates as a function of the PRF, R_p, if $R_p > 0.45\, B_{pf}$, with peak values touching the upper bound given by (11). Therefore, we use the upper bound (11) to formulate the SF. For $B_{pf} = 1$ MHz and 3 MHz the scaling factors are depicted in Fig. 14 which, for comparison, also shows the corresponding SFs $(B_{pf}/50\ \text{MHz})^2$ proposed by the FCC. For dithered signals we proceed in the same way by computing the SF on the basis of (12); the resulting curves for $B_{pf} = 1$ MHz and 3 MHz are also shown in Fig. 14.

The SF for DSSS (or DS-UWB) signals can be extracted from Fig. 9, by taking the maximum peak power value of the curves for $B_{pf} = 50$ MHz and $B_{pf} = 1$ MHz, see Subsection 5.5. The average PRF of this type of signals is $R_p = 1332.5$ MHz for a bit rate of 110 Mb/s pro channel; Fig. 14 shows the SF for this PRF which nearly equals the SF for dithered signals. This result was expected as DSSS is similar as 2PAM and because dithered and 2PAM signals have the same peak power for PRFs where $R_p > 10\, B_{pf}$, see Fig. 8.

The SFs for $B_{pf} = 1$ MHz and 3 MHz of a multiband-OFDM signal with a bit rate of 110 Mb/s are similarly extracted from Fig. 10; however, for OFDM signals no PRF is defined, therefore, the SFs are depicted as horizontal lines in Fig. 14. For multiband-OFDM signals and for the current FCC average- and peak power limits, a RBW of $B_{pf} = 3$ MHz is sufficiently large, such that the measured peak power P_p^m does not cause the peak power constraint to be active, i.e., the maximum allowed emitted PSD is not affected.

In Section 6 it is pointed out that the maximum allowed emitted PSD *does not depend* on the RBW, B_{pf}, for $B_{pf} \geq 1.875$ MHz and for the FCC's current average- and peak power limits (see Fig. 13(b)). This is because the average power limit is active instead of the peak power limit for $B_{pf} > 1.875$ MHz and $R_p \geq B_{pf}/2$. The range where $R_p > 1.875/2$ MHz is indicated by the shaded area in Fig. 14. For lower PRFs, our SF coincides with the factor $(B_{pf}/50\text{ MHz})^2$ (all three lines, *pulsed non-dithered*, *pulsed dithered*, and *FCC's SF* coincide).

Thus, for the FCC's peak- and average power limits, and for a RBW $B_{pf} \geq 1.875$ MHz the factor $(B_{pf}/50\text{ MHz})^2$ can be used instead of the SF in (22), to test UWB signals for compliance with the peak- and average power emission rules.

If, however, the FCC's peak power limit is changed such that the ratio $\hat{P}_p^m/\hat{P}_a^m$ is decreased by more than about 2.5 dB (see Fig. 13(b)), then for a RBW of $B_{pf} = 3$ MHz the peak power constraint is active for all PRFs, which results in a reduced maximum allowed emitted PSD. Therefore, in this case, the proposed SF in (22) should be applied.

8 Conclusion

This work investigates the impact of the average power and peak power constraints imposed by the FCC on the emitted power of UWB radio signals. Both, the average power and peak power are computed and/or simulated explicitly for different modulation schemes. This approach allows to closely reconstruct the results on the peak-to-average power ratio reported by the NTIA [3]. Furthermore, new insight on the requirements for achieving spectral flatness of UWB signals is obtained. Dithering has been proposed as a method to make the power spectrum of an UWB signal constant, i.e., "white", to make the corresponding signal less harmful to other systems; in this sense white noise is an ideal UWB signal. With respect to peak power, for example, Fig. 11 indicates that a white Gaussian noise signal has a similar peak power as dithered signals of the same signalpower (compare Figs. 8 and 11).

We have found that for a given UWB signal the peak power constraint being active or not can strongly depend on the RBW used to measure the signal's peak power. There is no real justification for the resulting disadvantage when using a RBW $B_{pf} < 50$ MHz, as the maximal

allowed peak power within a 50 MHz Bandwidth has been chosen based on the assumption that no victim receiver would suffer harmful interference from transmitting UWB devices. To determine the compliance of a UWB device with the FCC rules independent of the RBW, we propose to apply scaling factors that depend on the modulation details of the signal under test, or to consistently measure with a RBW of 50 MHz.

If, however, the current FCC's peak- and average power limits are applied, then the maximum allowed emitted PSD is independent of the RBW, B_{pf}, used to measure the peak power, for $B_{pf} \geq 1.875$ MHz. The FCC suggests a RBW of $B_{pf} = 3$ MHz. When the ratio of the peak power limit to the average power limit is decreased by more than about 2.5 dB, then the allowed emitted PSD depends on the RBW ,B_{pf}, even if $B_{pf} > 3$ MHz. In this case we propose to apply one of the two methodes described in Section 7 to determine the peak power level of UWB signals.

We have considered the peak and average power only for *in-band* emission (3.1 - 10.6 GHz). To consider out-of-band emission, the real shape of the emitted pulses must be considered instead of assuming Dirac delta pulses, furthermore, the peak- and average power levels must be evaluated at the corresponding out-of-band frequencies.

A Impulse Response of the Ideal Bandpass Filter

The impulse response $h(t)$ of an ideal bandpass filter with bandwidth B_f, computes form its equivalent lowpass impulse response $h_l(t)$ by

$$h(t) = \Re\left\{h_l(t)e^{i2\pi f_0 t}\right\}. \tag{23}$$

Zero passband attenuation implies that the energy of the filter impulse response is

$$\int f^2(t)dt = 2B_f. \tag{24}$$

Equation (23) can be shown to imply

$$\int f^2(t)dt = \frac{1}{2}\int |h_l(t)|^2 dt. \tag{25}$$

The lowpass impulse response $h_l(t)$ is given by

$$\begin{aligned} h_l(t) &= a\int_{-B/2}^{B/2} e^{i2\pi ft}df \\ &= \frac{a}{i2\pi t}\left[e^{i\pi B_f t} - e^{-i\pi B_f t}\right] \\ &= \frac{aB_f}{\pi B_f t}\sin(\pi B_f t) \\ &= aB_f \mathrm{si}(\pi B_f t), \end{aligned} \tag{26}$$

where a must be determined to satisfy (24). With (24), (25) and with

$$\frac{1}{2}\int |h_l(t)|^2 dt = \frac{1}{2}a^2 \int_{-B_f/2}^{B_f/2} df = \frac{1}{2}a^2 B_f$$

we have

$$\frac{1}{2}a^2 B_f = 2B_f \Longrightarrow a = 2,$$

thus (26) becomes,

$$h_l(t) = 2B_f \text{si}(\pi B_f t). \tag{27}$$

Using (23) we finally obtain

$$h(t) = 2B_f \cos(2\pi f_0 t)\text{si}(\pi B_f t). \tag{28}$$

B Peak Power Characterization of Gaussian Noise

We assume a Gaussian random variable u with Gaussian amplitude distribution and a root mean square (RMS) value, average power or variance denoted σ^2. The peak power p of u is defined as half of the instantaneous peak power value u^2, i.e., $p = u^2/2$ (compare the peak detector in Section 2). We determine the probability that the detected peak power p exceeds the threshold value p_t. By substitution, we find that

$$P(p > p_t) = P(|u| > u_t),$$

with $u_t = \sqrt{2p_t}$. The probability density function (PDF) of u is

$$f_u(u) = \frac{1}{\sqrt{2\pi}\,\sigma} e^{-\frac{u^2}{2\sigma^2}},$$

hence,

$$\begin{aligned} P(p > p_t) &= 2\int_{u_t}^{\infty} f_u(u)du \\ &= \text{erfc}\left(\frac{u_t}{\sqrt{2}\sigma}\right) \\ &= \text{erfc}\left(\sqrt{\frac{p_t}{\sigma^2}}\right). \end{aligned} \tag{29}$$

Table 1 contains probabilities $P(p > p_t)$ for certain threshold values p_t.

$P(p > p_t)$	10^{-1}	10^{-2}	10^{-3}	10^{-4}	10^{-5}	10^{-6}
p_t/σ^2	1.3527	3.3175	5.4138	7.5683	9.7557	11.9641
$10\log_{10}(p_t/\sigma^2)$ [dB]	1.3122	5.2080	7.3350	8.7900	9.8926	10.7788

Table 1: Value pairs satisfying (29).

References

[1] Federal Communications Commission (FCC). Revision of Part 15 of the Commission's rules regarding ultra-wideband transmission systems. *First Report and Order*, ET Docket 98-153, FCC 02-48, adopted on Febr. 14, 2002, released on April 22, 2002. [Online]. Available: http://www.fcc.gov.

[2] W. A. Kissick *et al.*, "The temporal and spectral characteristics of ultrawideband signals," [Online]. Available: http://www.its.bldrdoc.gov/pub/ntia-rpt/01-383, Jan. 2001, U.S. Departement of Commerce, NTIA Report 01-383.

[3] L. K. Brunson *et al.*, *Assessment of Compatibility Between Ultrawideband Devices and Selected Federal Systems*. U.S. Departement of Commerce, NTIA, January 2001, NTIA special publication 01-43.

[4] *Agilent Spectrum Analyzer Measurements and Noise, Application Note* 1303, Agilent Technologies, Inc., Feb. 2003.

[5] R. Kohno, M. Welborn, and M. Loughlin, "DS-UWB physical layer submission to 802.15 Task Group 3a," IEEE P802.15-04/0137r3, July 2004.

[6] A. Batra *et al.*, "Multi-band OFDM physical layer proposal for IEEE 802.15 Task Group 3a," IEEE P802.15-03/268r3, March 2004.

[7] Y. P. Nakache and A. F. Molisch, "Spectral shape of UWB signals - influence of modulation format, multiple access scheme and pulse shape," in *IEEE Vehicular Technology Conference (VTC)*, April 2003, pp. 2510–2514.

[8] United Kingdom, "Report of measurements to validate the assumption that UWB appears noise-like to a 3G terminal," TG3#2_35R0, May 2004.

[9] J. McCorkle, "DS-CDMA: The technology of choice for UWB," IEEE P802.15-03/277r0, July 2003.

[10] J. Tang and K. K. Parhi, "On the power spectrum density and parameter choice of multi-carrier UWB communications," in *Conference Record of the 37th Asilomar Conference on Signals, Systems and Computers*, vol. 2, Nov. 2003, pp. 1230–1234.

[11] OFCOM UK, "Interim report on issues relating to the modelling of UWB spectrum," UKTG1/8 (04) 37r1, July 2004.

[12] R. J. Fontana, "Petition for Reconsideration of Multispectal Solutions, INC." [Online]. Available: http://www.multispectral.compdfMSSI_022403.pdf, May 2003.